Multifunctional, durable and highly conductive graphene/sponge nanocomposites

Meng, Q., Yu, Y., Tian, J., Yang, Z., Guo, S., Cai, R., Han, S., Liu, T. & Ma, J.

Original citation & hyperlink:
Meng, Q, Yu, Y, Tian, J, Yang, Z, Guo, S, Cai, R, Han, S, Liu, T & Ma, J 2020, 'Multifunctional, durable and highly conductive graphene/sponge nanocomposites', Nanotechnology, vol. 31, no. 46, 465502.
https://dx.doi.org/10.1088/1361-6528/ab9f73

DOI 10.1088/1361-6528/ab9f73
ISSN 0957-4484
ESSN 1361-6528

Publisher: IOP Publishing

Multifunctional, durable and highly conductive graphene/sponge nanocomposites

Qingshi Meng[a, b], Yin Yu [a], Jiayu Tian [a], Zhaokun Yang[c], Shuang Guo[d], Rui Cai[e], Sensen Han[a], Tianqing Liu[f*], Jun Ma[a,g]

[a] College of Aerospace Engineering, Shenyang Aerospace University, Shenyang 110136, China

[b] Shenyang Aircraft Design Institute, Shenyang 110136, China

[c] Key Laboratory of Synthetic and Biological Colloids, Ministry of Education, School of Chemical and Material Engineering, Jiangnan University, Wuxi 214122, China

[d] Health Service Department, Northern Theatre General Hospital, Shenyang 110136, China

[e] School of Mechanical, Aerospace and Automotive Engineering, Coventry University, Coventry, UK

[f] QIMR Berghofer Medical Research Institute, Brisbane, QLD 4006, Australia

[g] School of Engineering and Future Industries Institute, University of South Australia, Mawson Lakes 5095, South Australia, Australia.

[*]Corresponding Author: Tianqing Liu; Email: michelle.tianqing.liu@gmail.com

Abstract

Porous functional materials play important roles in a wide variety of growing research and industrial fields. We herein report a simple, effective method to prepare porous functional graphene composites for multi-field applications. *Graphene sheets were non-chemically modified by Triton®X-100, not only to maintain high structural integrity but to improve the dispersion of graphene on the pore surface of a sponge. It was found that a graphene/sponge nanocomposite at 0.79 wt.% demonstrated ideal electrical conductivity. The composite materials have high strain sensitivity, stable fatigue performance for 20,000 cycles, short response time of 0.401s and fast response to temperature and pressure. In addition, the composites are effective in monitoring materials deformation and acoustic attenuation with a maximum absorption rate 67.78% and it can be used as electrodes for a supercapacitor with capacitance of 18.1 F/g.* Moreover, no expensive materials or complex

equipment are required for the composite manufacturing process. This new methodology for the fabrication of multifunctional, durable and highly conductive graphene/sponge nanocomposites hold promise for many other applications.

Key words: Multifunction; graphene; porous composites.

1. Introduction

Porous conductive materials have drawn great attention in electrochemistry, supercapacitor and microwave absorption fields [1-3] due to unique pore configuration, ultralight weight and conductivity [2, 4-6]. Traditional synthesis methods for conductive porous materials are summarized as the activation method which includes carbonized calcination [7-9], chemical, physical activation, catalytic activation [10-12] and aerogel preparation [13, 14]. The porous materials obtained by carbonization or calcination are brittle, almost non-flexible and have poor mechanical properties, which limit their applications. The activation process is complex, tedious and inefficient. The preparation process of aerogel is simpler than catalytic activation, but it requires chemical reaction, followed by freeze drying or annealing. In general, the materials obtained by the traditional method are often disordered, and it is difficult to control the shape and size of the pore channel [15-17], leading to limited structure stability, mechanical property and low functionalization. Therefore, we in this study select a sponge material [18-20], as it can be produced industrially on a large scale, has stable preparation technology and relatively regular pore structure as a scaffold for nanomaterials. In this way, the overall structural regularity [21-23] of composite materials can be improved as much as possible.

Graphene platelets (GnPs), which are highly crystalline few-layer graphene, have been widely used

as the conductive materials/filler to form porous conductive composites [24-27] for electronic applications due to excellent conductivity, compatibility and mechanical properties [28, 29]. Graphene/sponge composites are mostly fabricated by direct ultrasonic oscillation [30, 31], dip-coating layer-by-layer (LBL) electrostatic assembly [32] or adhesive [33, 34]. However, these fabrication methods may result in graphene aggregates in the sponge and detachment of the graphene materials due to either the limited dispersion of graphene in the solvent or the adhesion of polymers used. Therefore, it is of great importance to explore new strategies to prepare graphene/sponge nanocomposites to overcome the issues.

In recent years, piezoresistive sensors [35-37] with graphene as filler within sponge structure have been widely used in human motion detection, health monitoring, wearable electronic devices and human-machine interface, etc. For example, Passaretti, P., et al. [38] explored the interplay of the GraPhage13 structure formation and studies the mechanisms that give rise to the controllable self-assembly for applications in energy storage and conversion, catalysis and sensing. Lu, Y., Z. Niu, and W. Yuan [39] prepared multifunctional magnetic superhydrophobic carbonaceous (MSC) aerogel with hierarchically porous structures via a carbonization process using disposable cotton balls followed by surface-coating of Fe_3O_4 particles and post hydrophobic-modified treatment with long-chain silanes, which can be a good candidate for supercapacitors. Most of them are used in only two areas, and its single feature can be played in each area. This paper implements three different applications including engineering detection, sound insulation and electrodes for a supercapacitor. It is possible to combine two or more of these features and apply them to different fields.

In this work, we report a strategy to fabricate multifunctional, durable and highly conductive graphene/sponge nanocomposites (GSC) by forming 3D conductive nanostructures using a sponge as

the skeletons and graphene platelets (GnPs) as the filler. *The physical modified GnPs are used as the filler to maintain the overall structural regularity of the composite to the greatest extent, thus improving its mechanical and electrical properties. The tripolycyanamide sponge material used also has good porosity and pore size characteristics, thus optimizing the overall structure of the composite material.* The effects of filler concentration of the composites on their responses to mechanical deformation (compression and strain), electrical properties, sound insulation and capacitance properties are investigated in details. *The resulting nanocomposite exhibits high flexibility, lightweight, excellent sensing capacity and outstanding reliability and stability during the long-term fatigue performances. We demonstrate potential applications of this sponge composite as a multifunctional sensor for mechanical deformation monitoring, sound absorption/attenuation for aircraft and electrodes for a supercapacitor.*

2. Experimental section

2.1 Materials and Chemicals

Graphite intercalation compound (GIC, 1395) was kindly supplied by Asbury Carbons (USA). *The melamine sponge (tripolycyanamide) with the density of 15-17 kg/m^3 was provided by Xijie Co. (China). The porosity was 88.725% ± 0.53%.* Triton®X-100 was purchased from BioFroxx (Germany). All materials were supplied without further purification.

2.2 Fabrication of multifunctional graphene/sponge nanocomposite (GSC)

Graphene platelets (GnPs) were prepared using our published method [24, 40, 41]. In brief, 1 g of a graphite intercalated compound (GIC) was transferred into a preheated crucible placed in a furnace at 700 °C for 1 minute, and it was left to cool in air to obtain expanded product. The product was

mixed with acetone and further processed for ultrasonication for approximately 2 hours below 25°C. Finally, the solution was dried in a vented oven to obtain GnPs.

A piece of sponge (2.00 × 2.00 × 0.25 cm) was used as the *scaffold* in this study. The preparation method is illustrated in Figure 1 using the 0.79 wt.% GnPs/sponge composite sample as an example. GnPs (0.5 g) and 5 mL of Triton X-100 were mixed together in an agate vessel for about 40 min. Deionized water (63 mL) was then added and the mixture was stirred using a mechanical stirrer for 2 h. The sponge was emerged into the solution within a beaker under sonication for 10 h in order to allow the modified GnPs to fully infiltrate into the sponge skeleton. The graphene/sponge composite was dried in an oven at 75°C.

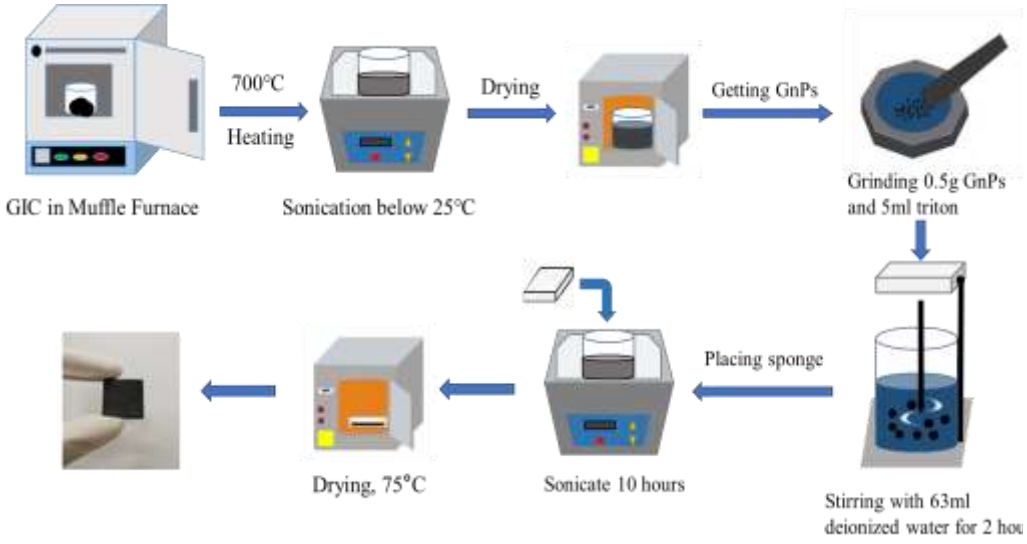

***Figure 1**: The schematic of preparation for a multifunctional, durable and highly conductive graphene/sponge nanocomposite*

2.3 Fabrication of sample for capacitive properties

Two sponge electrodes (6.00 × 2.00 × 0.25-0.27 cm) were immersed in 1 M Na_2SO_4 solution overnight. Then, a sandwich structure was created by combining the electrode sponges, two pieces of

platinum sheets as the current collectors and a piece of filter paper as the separator.

2.4 Characterization

A graphite intercalation compound (GIC) was placed in acetone and then treated with ultrasound for 5 h. Finally, the solution was diluted for three times to obtain samples for TEM. GnPs were prepared on 200-mesh copper grids and imaged using a high magnification transmission electron microscope (TEM, *JEM-2100, JEOL, Japan)* at 200 kV. The surface of the composite was observed by a scanning electron microscope (SEM, *SU8010, Hitachi, Japan*) with an accelerating voltage of 5 kV. *Raman spectra of GnPs were obtained by a Raman spectrometer Avantes AvaRaman (The Netherlands).* A small piece of the composite was prepared by cutting from the composite and coated with a thin layer (10–20 nm) of platinum prior to SEM imaging.

The electrical conductivity of the composite was measured by a square resistance meter (*Daming, DMR-1C*) with the measuring range of 20 Ω (220 V AC, 0.1 A). In a typical measurement, the probe of the square resistance meter was carefully placed on the surface of the composite material with an appropriate range selected for reading, and finally it was converted to conductivity.

Tensile strength of the composite was evaluated using a universal tensile machine *(GX-SF001, Shenzhen Shared instrument equipment co. LTD, China)* with the strain rate of 2 mm/min at room temperature (25 ℃). The overall sample size was 6.00 × 2.00 × 0.25–0.27 cm with a gauge length of 35 mm. At least three samples were used to obtain an average for all measurements and calculations.

Fatigue test was conducted using a universal tensile machine *(GX-SF001, Shenzhen Shared instrument equipment co. LTD, China)* at a strain rate of 50%, and the testing range was selected as 50% of the sample's elongation at break. 20,000 cycles are tested at 3.33 Hz. *A FLUKE 2638A hydra*

series III data acquisition device was used to constantly monitor the resistance of the composite material during fatigue tests.

For the data processing of sound-absorbing/attenuation experiment, Magic Music Editor Software was used to collect decibel values. The voice frequencies with MP3 format of the collected three controlled trials were turned on in the software and the absorption rates were calculated according to the displayed decibel value.

An electrochemical workstation (*CHI660E B19038, Chenhua Instrument CO., Shanghai, China*) was used to analyze the capacitive properties of the multifunctional graphene-based composite sponge.

3. Results and discussion

3.1 Characterization of GnPs

The morphology of GnPs was observed by TEM. Figure 2a shows that GnPs have a large specific surface area with overlapped structure, which makes the conductive path wider. This structure can potentially improve the overall electrical conductivity of the material. The enlarged image showed that the sheet edge is featureless, almost transparent and thin, indicating the possibility of being a monolayer graphene (Figure 2b). The morphological study shows that GnPs possess a thin two-dimensional structure, and the sheets are stable even when they were exposed to the electron beam during TEM tests. *The Raman spectra of GnPs (Figure 2c) show that GnPs have significant absorptions at 1362, 1584 and 2723 cm^{-1}, corresponding to the D, G and 2D bands, respectively. The G band refers to the sp^2 resonance on an ordered graphite lattice, while the D band is activated by substituted in the plane heteroatoms, vacancies, grain boundaries or other defects through the first-order scattering process of sp^2 carbon. These defects may be sp^3 hybridized carbon structure, which*

is related to the amount of impurities or the degree of oxidation. Since all samples were tested in a powder form, there is no need to discuss the 2D band.

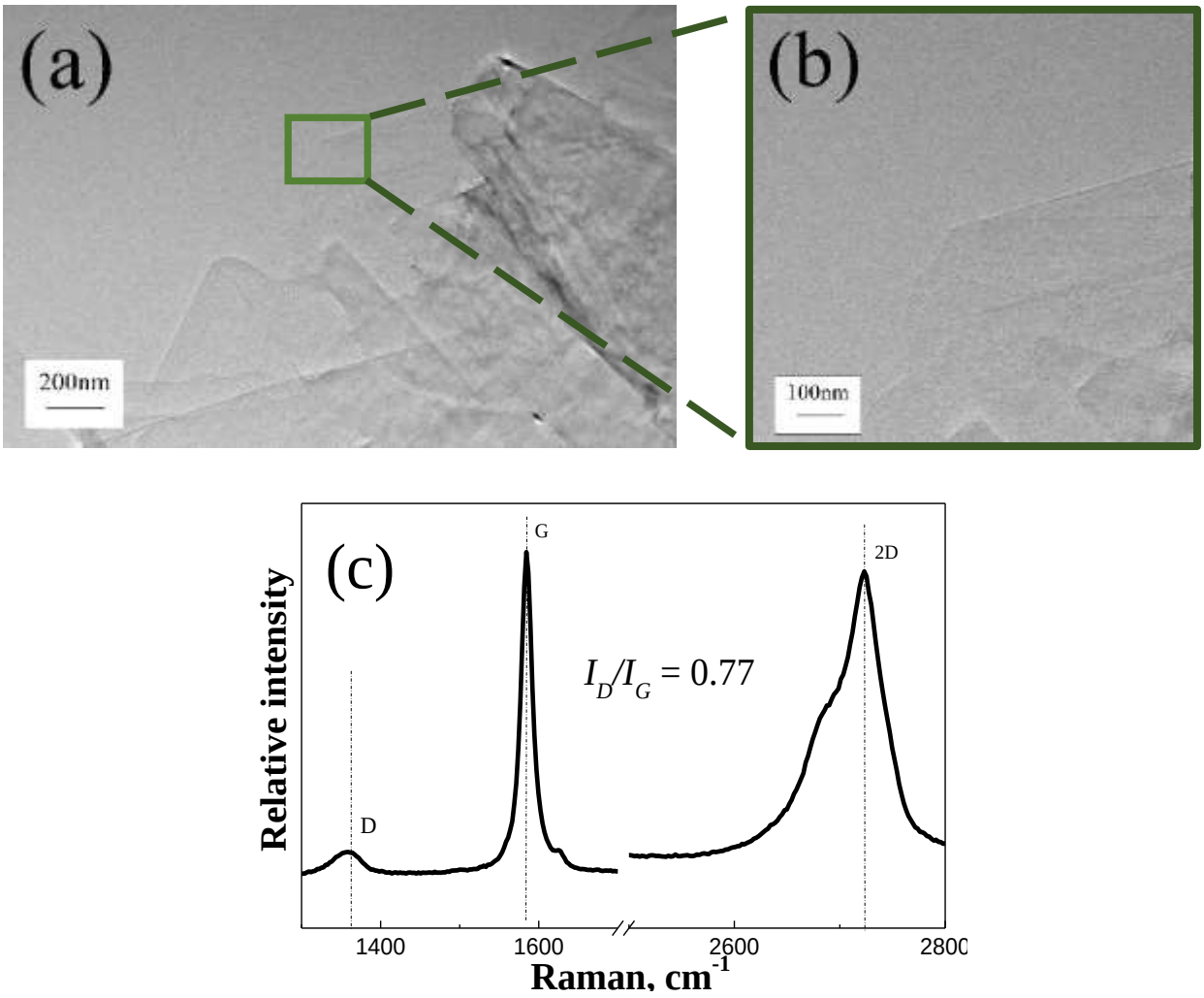

***Figure 2**: (a & b) The TEM images of graphene platelets (GnPs) and (c) Raman spectra of GnPs.*

3.2 Morphology of multifunctional, durable and highly conductive graphene/sponge nanocomposite (GSC)

The morphologies of three different sponge systems including pure sponge without GnPs, sponge with the unmodified GnPs and sponge with the modified GnPs are compared by using SEM (Figure 3). All the sponges possess the 3D interconnected and cellular-like porous networks, which could potentially provide mechanical backbone for the fillers. Figure 3a1 shows a typical smooth sponge

structure without the presence of GnPs. The internal porous network structure with the pore size of 2–3 μm can be clearly observed in Figure 3a2. However, it can be seen from Figure 3b1 and 3b2 that the unmodified GnPs (0.79 wt.%) are not well dispersed within the sponge structure due to lack of modification by Triton. Visible aggregates consist of a great number of irregular GnPs at the junction of the sponge skeleton (Figure 3b2). Figures 3c1 and 3c2 illustrate SEM images of the graphene/sponge composite containing the modified GnPs with Triton®X-100. Compared with Figure 3b1, the modified GnPs are more evenly dispersed within the sponge. These GnPs at 0.79 wt.% are densely coated and randomly interconnected on the sponge skeletons, resulting in the formation of a thin conductive layer (Figure 3c2).

Figure S1 compares the suspension time of the modified graphene sheets with those unmodified in solvent, demonstrating that the modified sheets disperse better. Most graphene sheets are stacked on top of each other, while some graphene sheets protrude from the surface. The interfacial interactions between GnPs and sponge are crucial in determining the final performance of the composites. These thin and uniform graphene sheets can be more evenly attached to the sponge skeleton to form a 'coating' structure, which would improve the mechanical properties of the sponge skeleton. However, the unmodified graphene sheets tend to form more aggregates inside the sponge, resulting in irregular interface structure. The aggregates can affect the mechanical properties, electrical conductivity and other properties of the resulting composites. Therefore, the modified GnPs are selected for the following studies. *Using ImageIJ image recognition software, the pore diameter of the sponges is calculated to be 65.6±20.1 μm.*

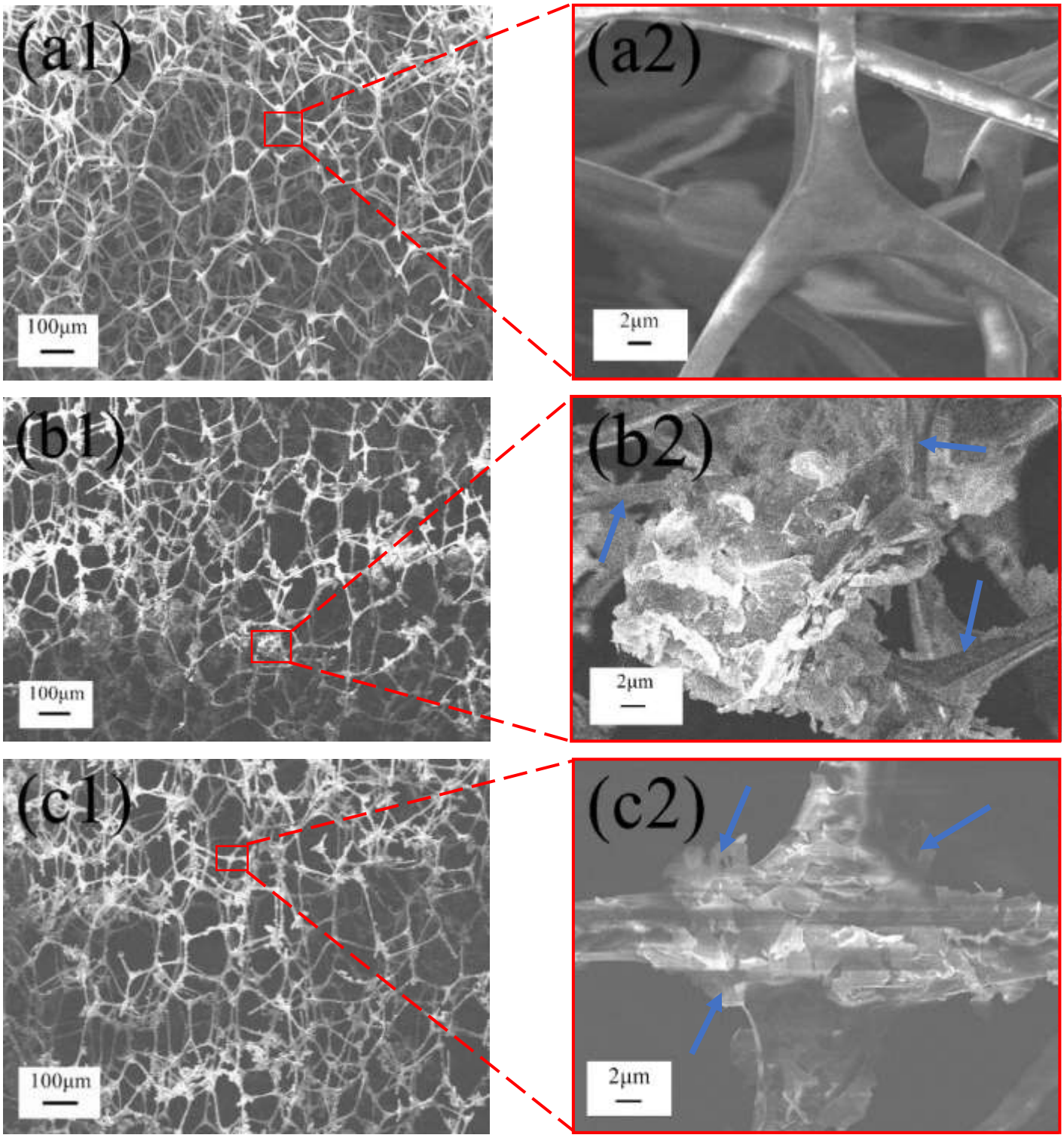

Figure 3: The SEM images of (a1 & a2) pure sponge without any filler, (b1 & b2) sponge with unmodified GnPs and (c1 & c2) sponge with modified GnPs

3.3 Electrical conductivity

The electrical conductivity of the graphene/sponge nanocomposite is influenced by the dimension of GnPs and their interfacial bonding with the sponge skeleton. The low thickness of graphene sheets achieved by longer sonication time can make these easier to adhere to the sponge skeleton and to obtain higher electrical conductivity. We randomly select three samples with different fractions of GnPs, i.e., 0.47 wt.%, 0.79 wt.% and 1.27 wt.% with sonication treatment of 6, 8 and 10 hours, respectively. In Figure S2a in the Supporting Information, the composite conductivity increases with the treatment time. Therefore, we use 10 h as the optimum sonication time for the preparation of the composites.

The composite conductivity presents a wavy trend with at filler fractions 0.47 – 1.27 wt.% (Figure 4). It obviously rises at 0.47 – 0.79 wt.%, likely because no visible agglomeration occurs at the range. As the GnP content increases to 1.11 wt.%, some agglomeration may form in the sponge, which leads to uneven internal structure within the composite and thus affects the conductivity. At over 1.11 wt.%, the conductivity increases gradually, and this means that such graphene at such a high fraction would form more conductive pathways.

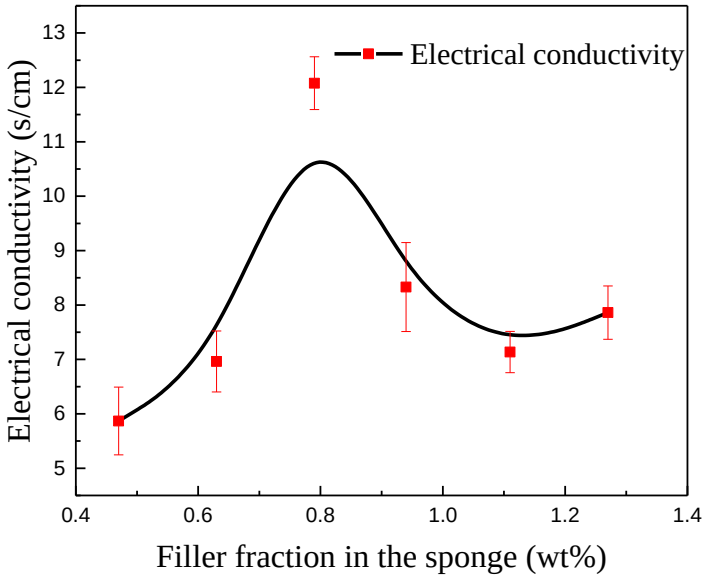

Figure 4: Electrical conductivity with different filler fractions in sponge

3.4 Mechanical property

3.4.1 Tensile strength and elongation at break

Figure 5 shows the tensile strength and elongation at break of the graphene/sponge nanocomposites. Higher GnPs can enhance the tensile strength but elongation at break decreases. The maximum tensile strength of 0.232 MPa was achieved at 1.27 wt.% of GnPs with an increment by ~35%. The minimum elongation at break of 5.667% is achieved at 1.27 wt.%, a reduction by ~66.9 %, while the maximum elongation at break of 17.22% is achieved without GnPs. The reduction is due to the increase in the rigid and high-strength phase (GnPs) in the composite. In Figure 5, two curves meet at 0.79 wt.% where tensile strength and elongation at break are generally accepted in practice.

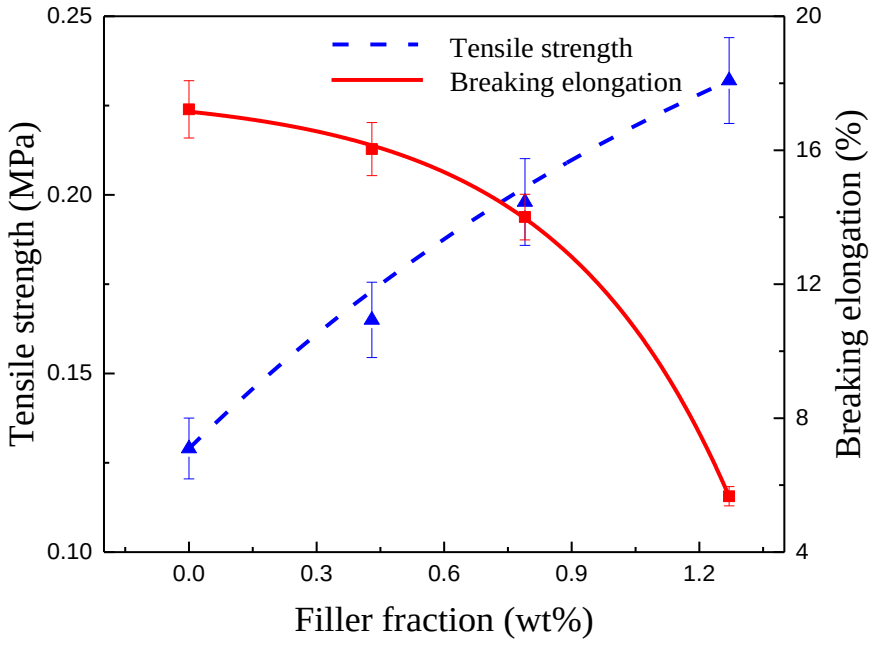

Figure 5: Tensile strength and elongation at break of the sponge nanocomposites

Based on the above analysis of electrical and mechanical properties, the nanocomposite at 0.79 wt.% has demonstrated not only the highest conductivity but a balance between tensile strength and elongation at break. Therefore, the sample at 0.79 wt.% is selected as the representative for the following measurement.

3.4.2 Strain fatigue property

It is critical to investigate the durability and stability of the nanocomposites by repeatedly stretching-unloading cycles under 0.5 mm strain for 20,000 cycles at a frequency of 3.33 Hz. The relative resistance change ($\Delta R/R_0$) is recorded as shown in Figure 6. The composite has shown satisfactory stability, because the gradual attenuation of $\Delta R/R_0$ occurs with very minor resistance variation.

In comparison with other measurements with fewer cycles [42-47], this experiment adopted more cycles to show long-term performance of the nanocomposites. The enlarged images show that the lowest $\Delta R/R_0$ -0.034 happens at the initial 0–200 cycles, which decreases to -0.048 at 19,800–20,000

cycles. This is because the composite has not reached a stable state in the early stage but its performance tends to be stable after the first 200 cycles. The obvious relative resistance decreases can be observed after 20,000 cycles due to the change of stable conductive network during dynamic loadings [48, 49]. In the last 200 cycles, the sponge is slightly deformed after a large number of stretch cycles leading to changes in the internal conductive network structure and thus a gradual decline in the resistance change rate. However, the resistance change with stretching is nearly consistent over thousands of cycles, which suggests promise applications for long term applications..

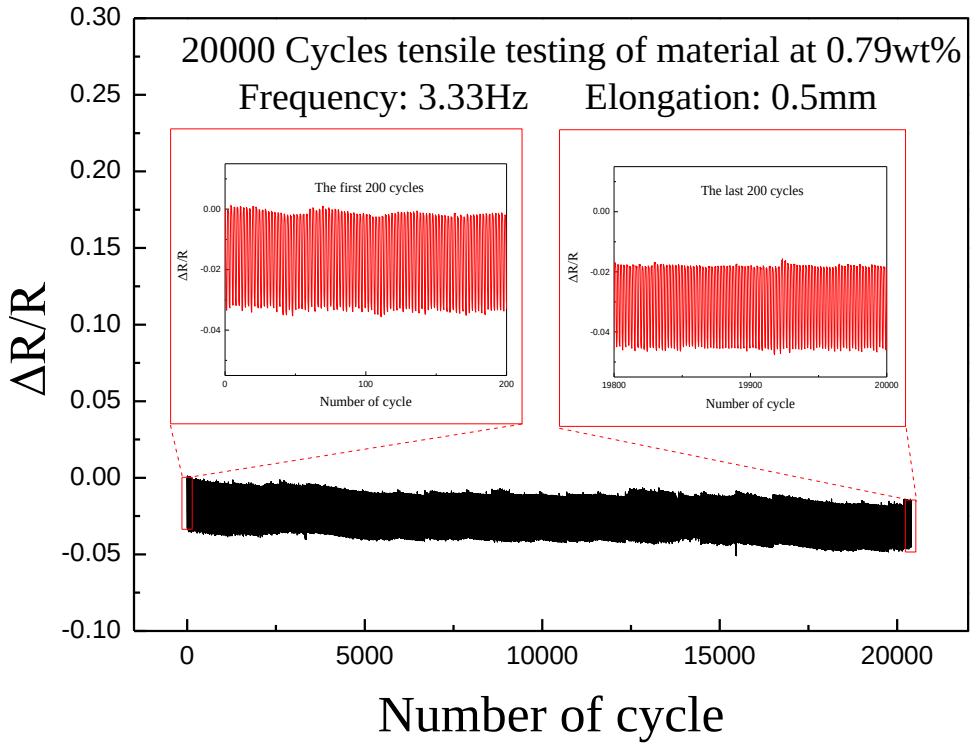

Figure 6: Strain fatigue test

3.5 Stretch linearity

Signal linearity is normally required for high-performance strain sensors to achieve accurate signals. During longitudinal stretching, the cross-section area of the composite was reduced by compression.

When the composite material was deformed in the stretching direction, the cross section shrank. Then the inter-distance between GnPs would decrease resulting in denser conductive paths, as shown in Figure 7a, which caused the resistance decrease. Figure 7b shows the relative resistance change ($\Delta R/R_0$) under a series of strain (0 – 15.565%). The variation rate of resistance decreases uniformly with increase in strain, which indicates that the composite has a good linearity. The gauge factor (sensitivity) was measured to be 0.01 (from 0 – 15.565%). *The stress-strain curve can be seen in Figure S3 in the Supporting Information.*

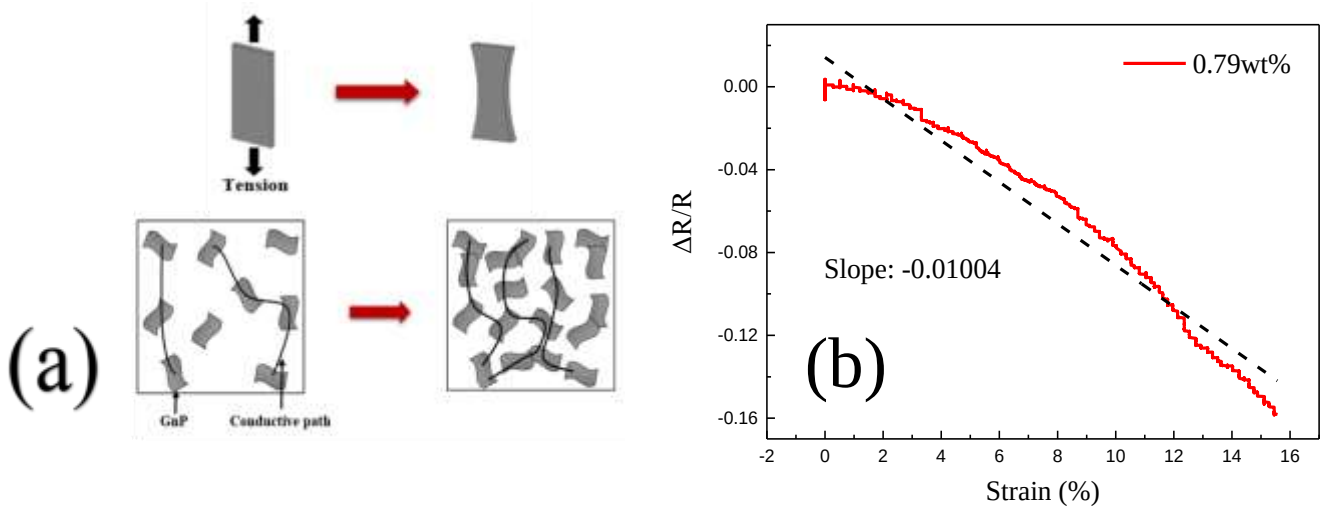

Figure 7 (a) Stretch principle diagram and (b) stretch linearity

3.6 The flexible analysis

To test the flexibility of the graphene/sponge nanocomposites, the resistance change was investigated under different mechanical loadings, including bending and torsion. Figure 8 shows significant change in resistance at different bend angles and twist angles. The composites have shown good flexibility by being able to withstand the aforementioned loadings without permanent deformation (tearing). It can be clearly seen that the resistance decreases with the increase of angle, suggesting

their potential for detection of angular deformation as a strain sensor.

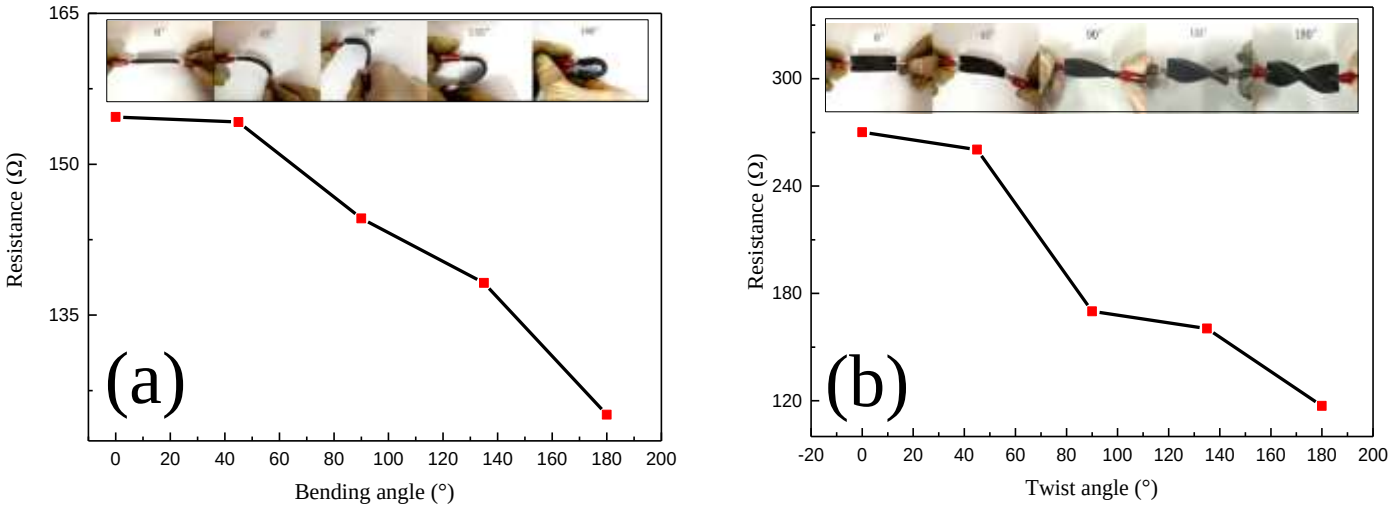

Figure 8: The resistance variations with different bending angles and twist angles

3.7 Pressure sensitivity

To investigate the pressure sensitivity of the composite, weight loads of 2.45 KPa, 4.90 KPa and 12.25 KPa are applied to the composite at the same time interval to observe the change of resistance. In Figure 9a, when the pressure acts on the composite, the internal structure of the composite becomes dense leading to increased density of the conductive network and improved conductivity. It can be seen that the composite has a relatively short reaction time under 2.45 KPa (Figure 9b). Figure 10c compares the deformation before and after the pressure loading. The composite can maintain basic structure under a range of pressure. As seen from Figure 9d, with the continuous increase of pressure, the composite resistance changes significantly. The expected reason is that when the upper and lower layers of the conductive framework are closely packed under higher pressure, the dense conductive channels can be formed, which leads to more resistance change under the compression pressure. The most significant resistance change is achieved under the load of 12.25 KPa. In addition, the trend of

the resistivity change curves is consistent under different pressures, which can reflect the resistance stability and excellent pressure sensitivity of the composite.

Figure 9 (e) reveals the stress-strain graph of the nanocomposite showing a maximal compressive strain of 92%. Similar to other porous materials [48, 50], the graph can be divided into three typical regions: a nearly linear elastic region at strain < 10%, a relatively flat plateau at 10 – 60% and a stress increasing region at 60 – 90%. In the first region, the composite deforms linearly with stress, and this elastic region is followed by a plateau from 10% to 60% with buckling of the scaffold as well as the partially collapse and irreversible damage. In the abrupt stress increasing region, with the densification of GnPs, the composite is crushed together and behaves like bulk materials, leading to significantly higher stress. The maximum strain can be up to 92%.

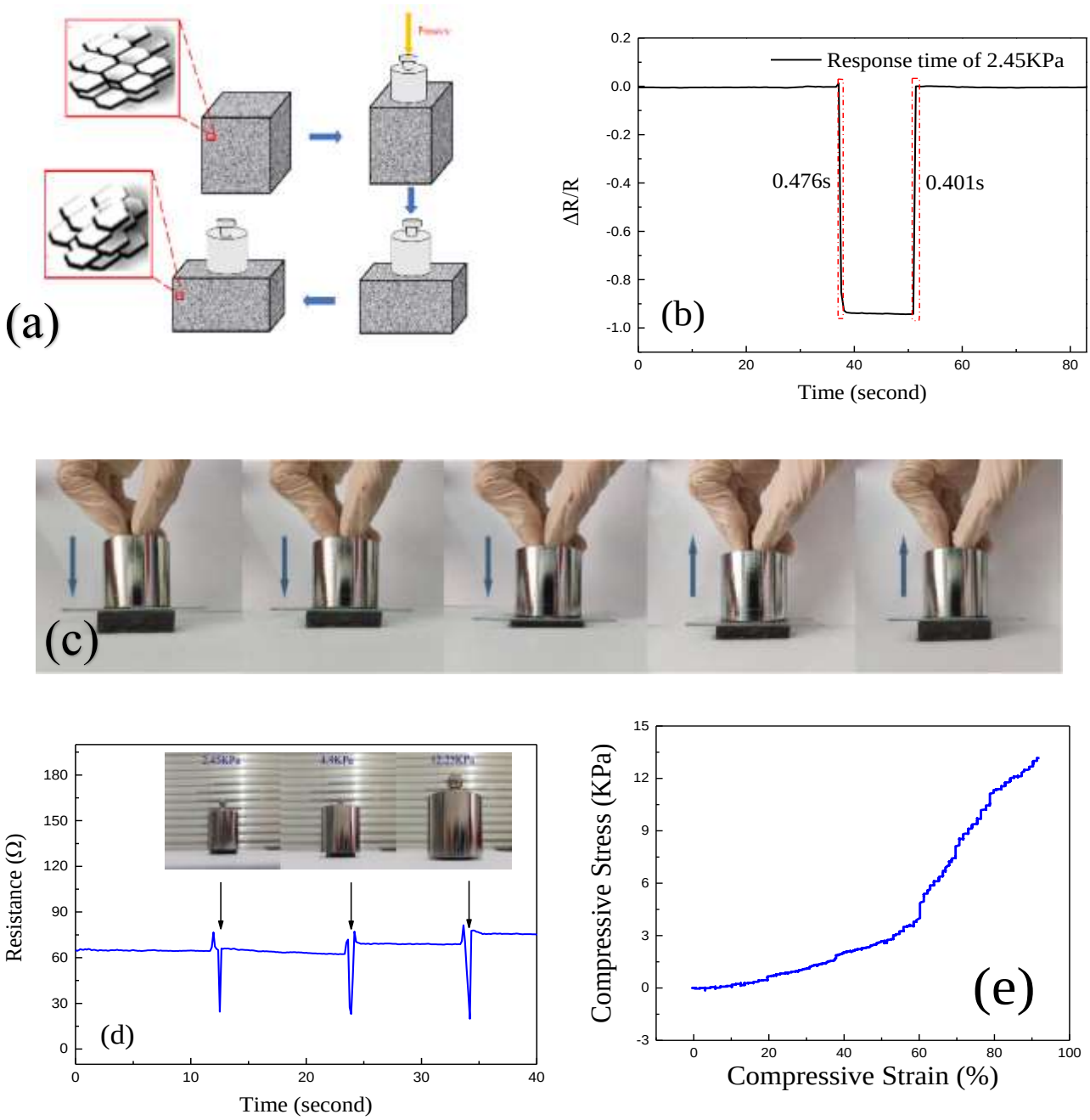

Figure 9: (a) Schematic diagram of compression, (b) compression response time, (c) resilience diagram, (d) the pressure sensitivity testing of the composite and *(e) compressive stress–strain curve with a maximum strain of 92% for the composite.*

3.8 Temperature response

Temperature drift generally refers to a fact that the change of ambient temperature causes the change of the semiconductor or conductor sensing parameters leading to scattering of output signals. It is

necessary to explore the effect of temperature on the conductivity of the graphene/sponge nanocomposite. *The temperature response test was conducted over a temperature range of 35 – 90 ℃ with an increase rate of 54.55 second/℃. As can be seen from Figure 10, the resistance of the composite increases with temperature. In the process of 0 ~ 54 ℃, the resistance rate increases; after 54 ℃, the rate decreases, and it gradually becomes stable at higher temperature.* The result shows that composite is sensitive to temperature changes in the specific temperature range, indicating its potential as a temperature sensor.

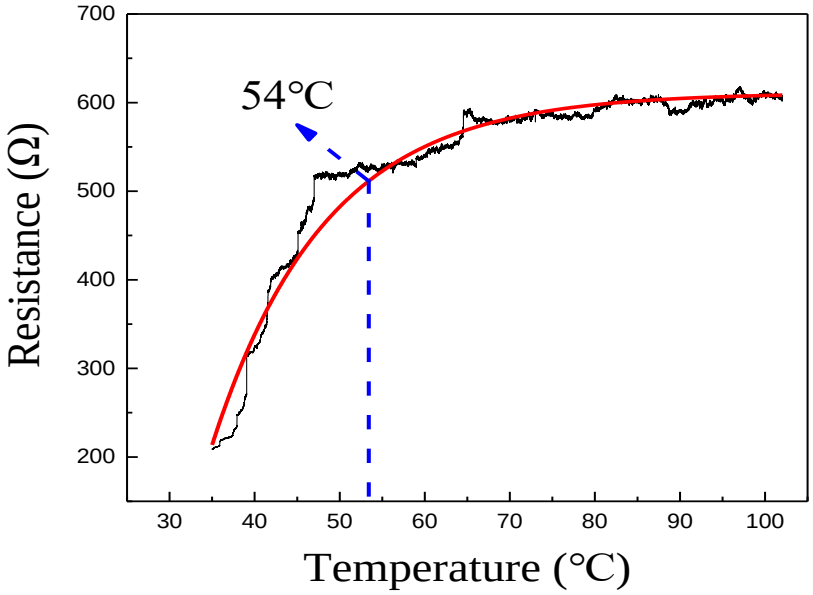

***Figure 10**: The change of resistance with temperature*

3.9 Application

3.9.1 Deformation monitoring

Since the composites have excellent flexibility, reliability, durability and sensitivity, they are suitable for monitoring the deformation of beam frame in engineering. To set up a deformation monitoring test, an stainless steel ruler was used to simulate the beam structure (Figure 11a-c). The composite was attached to the beam without warping under different structural changes, which provided close

contact between the composite and the beam. Figure 11d shows that when the ruler is in the neutral state, the change of resistance is stable at approximately zero. However, when bending occurs, the resistance signal demonstrates an obvious change, suggesting that it can more accurately and efficiently detect real-time deformation. This particular response to deformation provides a basis for applications in structural engineering.

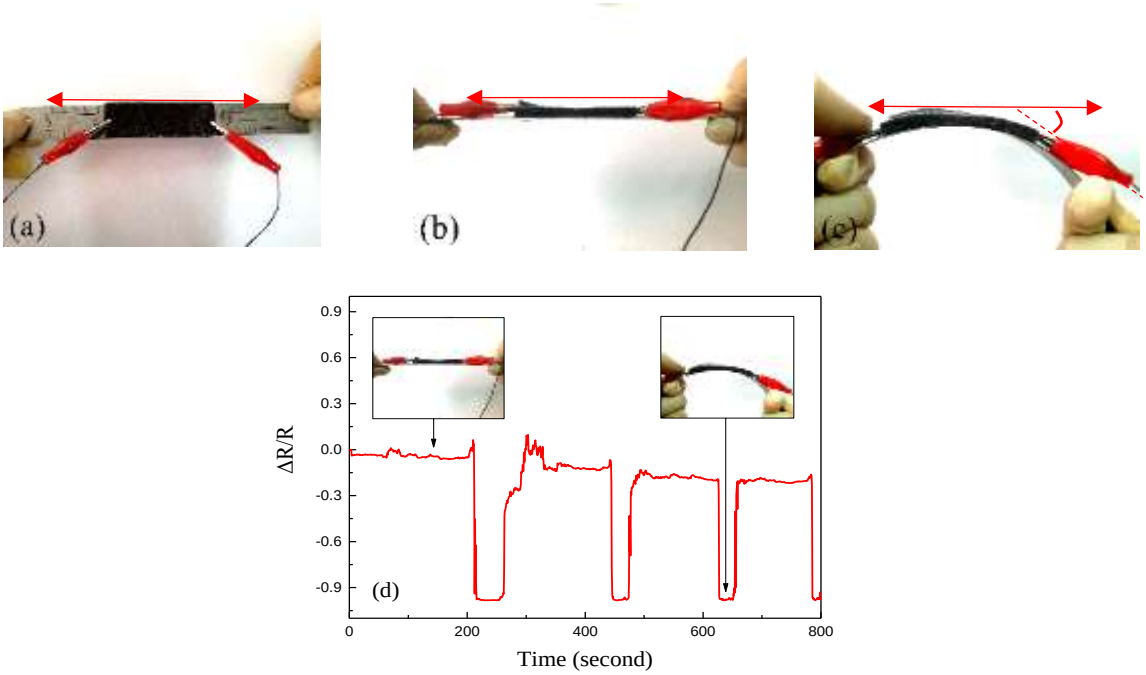

Figure 11: (a-c) Conformability between a composite and a beam and (d) the rate of resistance change under different deformation

3.9.2 Sound absorption performance

Porous materials are commonly used for sound insulation and noise reduction. Here we investigate the acoustic absorption performance of a graphene/sponge nanocomposite at 0.79 wt.% of GnPs. In Figure 12a-d, the sound absorption is compared by recording the audio frequency obtained from the music players in three containers. Figure 12e (1-3) shows the research method where a container is surrounded by many pieces of the nanocomposite in comparison with both an empty container and a

container with pure sponges. In Figure 12f, the nanocomposite container reveals the best sound absorption effect. For high decibels, the absorption rate of empty box is 46.67%, that of box filled with pure sponges is 55.56% and that of box filled with graphene/sponge nanocomposites is 63.33%. For low decibels, the absorption rate of empty box is 55.56%, that of box filled with pure sponges is 56% and that of box filled with graphene/sponge composites is 67.78%. The results indicate the composites have superior sound absorption capability.

The results show that the irregular shape of GnPs on the sponge skeleton increases surface roughness causes the diffuse reflection effect, which is scattering of the reflected wave in multidirectional to promotes sound-absorbing effect. Hence, the composites can be used for sound attenuation in military focused vehicles, such as aircraft and submarine, where stealth is of utmost importance.

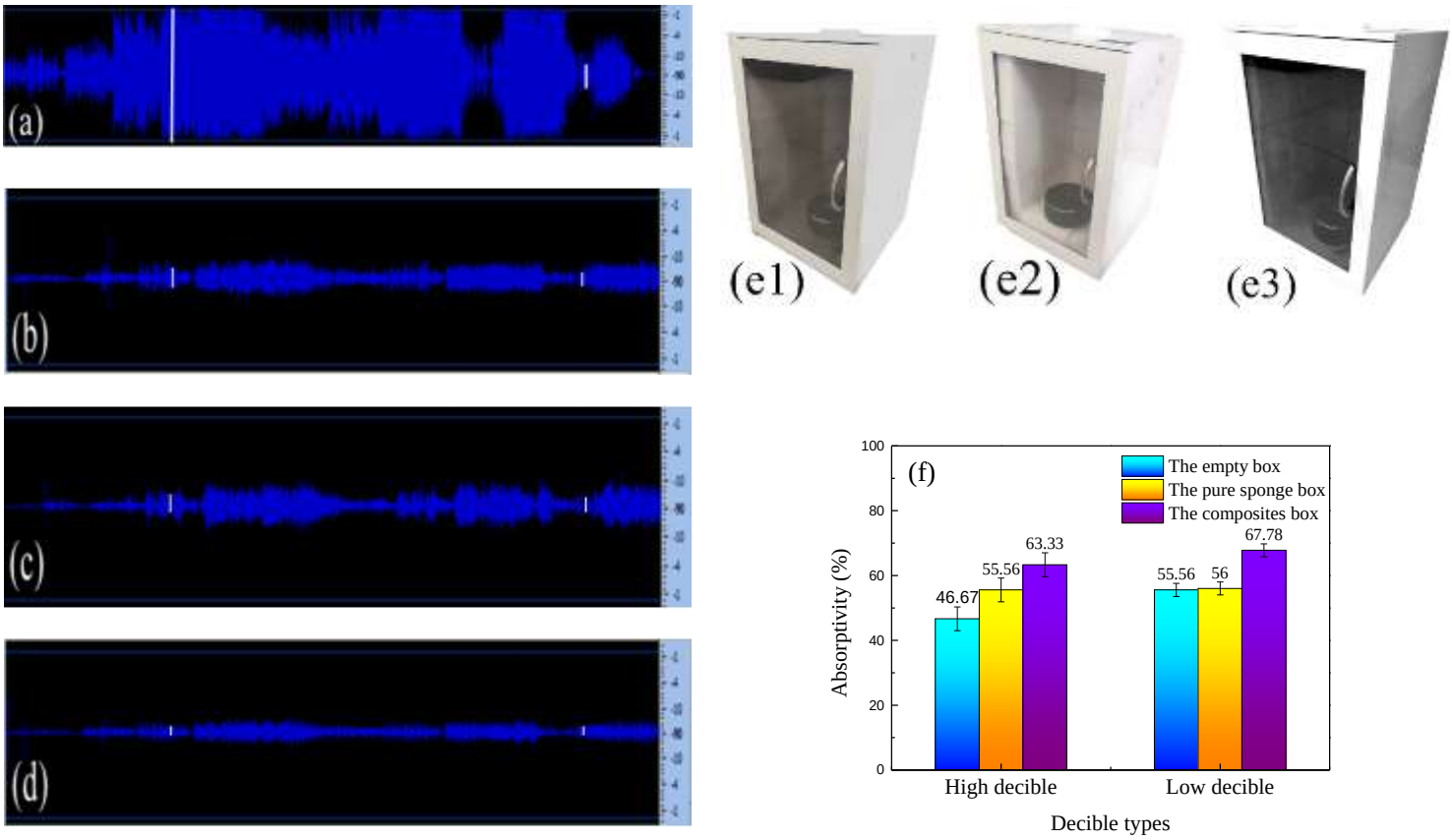

Figure 12: (a-d) Audio in different dark rooms, (e1-3) the darkrooms and (f) acoustic absorption at different decibel

3.9.3 Supercapacitor

As discussed above, the graphene/sponge nanocomposites are electrically conductive and porous, making it applicable in supercapacitors. The electrochemical performances of the composite electrodes are studied by cyclic voltammetry (CV) and galvanostatic charge/discharge (GCD). In Figure 13a, two methods were used to fabricate the supercapacitors. One is to take the composites as the electrodes and separate it with filter paper to form the two-electrode system. The other approach involves coating graphene sheets above and below the sponge, so that the uncoated sponge in the middle acts as a medium to form a two-electrode system. Since the first method can better reflect the application of supercapacitors, it was used in this study.

Figure 13b shows the CV graphs at a scan rate of 100 mV/s within 0 – 0.8 V. For composites with pure sponges, CV curve is a straight line, implying no electrochemical capacitance. In contrast, the CV curve of graphene/sponge nanocomposites approximates to a leaf-like parallelogram, indicating a typical supercapacitor characteristic. This feature is contributed by GnPs, because of high electrical conductivity and oxygen-containing groups [51].

Since the performance of supercapacitors is related to the content of active substances in the materials, we compared the CV images for the nanocomposites at 0 wt.%, 0.63 wt.%, 0.79 w.t% and 1.27 wt.%. The CV curve of the 0.79 wt.% graphene/sponge nanocomposites is less uniform and out-of-shape than others, but it has larger area representing the highest specific capacitance. The reason is that the graphene/sponge composite with a high filler fraction creates more electron pathways and offer more interface for energy conversion. The specific capacitance values calculated from CV curves are 8.3, 9.9 and 7.5 F/g, respectively for the nanocomposites containing 1.27 wt.%, 0.79 wt.% and 0.63 wt.% of GnPs. The capacitive property decreases gradually after 0.79 wt.%. This is due to the agglomeration of graphene sheets under high packing composition, which reduces the ability of carrying electrons and ions. Therefore, we focus on the 0.79 wt.% composite.

We specifically investigate the performance of the 0.79 wt.% graphene/sponge nanocomposite at 20 – 100 mV/s. In Figure 13c, the shape of the cyclic voltammetry (CV) curves is similar to parallelogram at different scan rates. The specific capacitances calculated from the CV curves are respectively 18.1, 11.1 and 9.9 F/g when the scan rates increases from 20 mV/s to 100 mV/s. The graphene/sponge nanocomposites show a slight reduction in specific capacitances with increasing scan rate.

In Figure 13d, the specific capacitances calculated from the charge/discharge curves are respectively 15.8, 15.0, 12.0 and 7.5 F/g at different current density (from 0.5 to 5 A/g). It is obvious that the discharge time decreases with increase in current density and the capacitance decreases with increment in either scan rate or current density. The trends are due to the fact that the electrode materials cannot get instantaneously charged since the diffusion of protons within the electrode materials is time dependent. The specific capacitance ranges respectively calculated by CV diagram and GCD are approximately the same.

Figure 13e shows that capacity retentions are 94.3% for the graphene/sponge nanocomposite at 0.79 wt.%. The cyclic testing shows a high capacitance because GnPs act as a good electron shuttle resulting in more stable electrodes. The small decrease in specific capacitance can be attributed to the microstructural changes caused by small expansion and contraction deformation of graphene sheets during charge and discharge. The long-term cyclic testing shows high stability for the supercapacitor based on graphene/sponge nanocomposites.

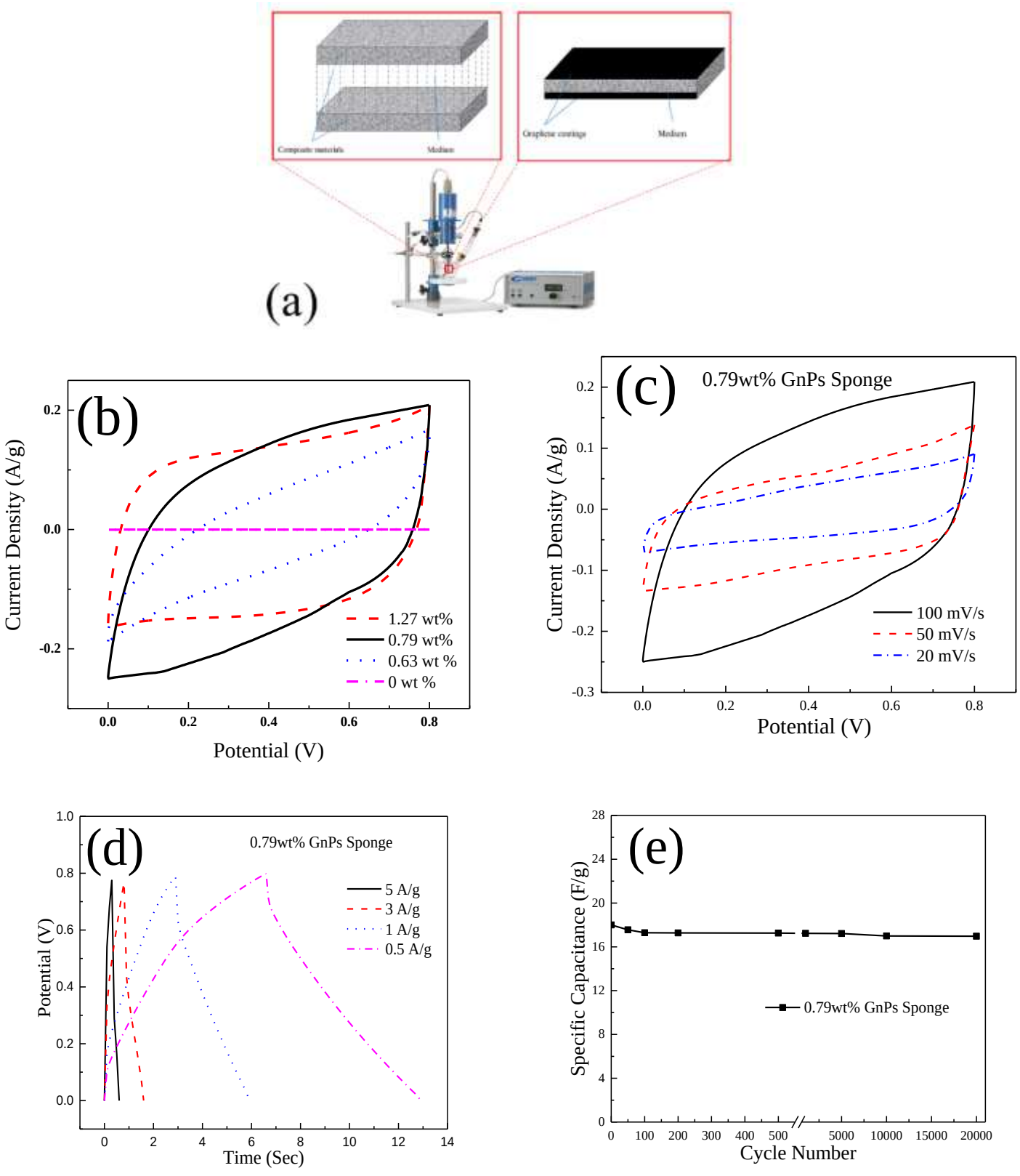

Figure 13: Electrochemical characterization of supercapacitors based on graphene/sponge composites containing 1.27wt%, 0.79wt% and 0wt% graphene sheets (GnPs): (a) Schematic diagram of supercapacitor, (b) CV curves obtained at 100 mV/s, (c) CV curves at various scan rate , (d) GCD curves of the 0.79wt% graphene/sponge composites and (e) cyclic stability

It is worth discussing the advantages of the choice of scaffold and the method of modification graphene sheets *[32, 43-45, 52-56]*. As seen in Table 1, in terms of the size of sponge skeleton, our sponge has smaller diameter and higher porosity, which is conducive to adhesion of more graphene sheets to the skeleton scaffold. Due to this, the diffusive reflection effect of sound waves inside the composite material is more effective, thus improving sound attenuation.

Table 1: Comparison with different sponge composites

Material	Skeleton diameter	Dispersion of filler	Others	References
CB/STG-PU	About 20-30 times larger	Nonuniform	N/A	[44]
RGO-PU	Almost similar		Transformation	[43]
MWCNTS-PU	About 50 times larger	Nonuniform	N/A	[32]
MWCNTS-RGO-PU		Nonuniform	N/A	
RGO-PU		Uniform	N/A	
NDs-fPDA-PU	About 20-30 times larger	Nonuniform and agglomeration	N/A	[52]
3-Mercaptopropyl-GO-PU	About 20-30 times larger	Nonuniform	N/A	[45]
CNT-CS-PU	About 10-20 times larger	Nonuniform	N/A	[53]
RGO-PU	About 10-15 times larger	Nonuniform	With adhesive	[33]
rGONR-PU	*About 10 times larger*	*Uniform*	*N/A*	*[55]*
GOWR-MF	*About 2 times larger*	*Uniform*	*N/A*	*[56]*
RGPS	*About 2-3 times larger*	*Nonuniform*	*N/A*	*[54]*

Please refer to the Annotation in the Supporting Information for abbreviations in table.

Conclusion

In conclusion, we proposed a simple yet effective method to prepare multifunctional, durable and highly conductive graphene/sponge nanocomposites for multi-field applications. *By modifying graphene and adjusting its fractions, we optimized the composite structure for high sensitivity, stable fatigue performance, less response time and ideal responses to temperature and pressure. In addition, the composites have demonstrated remarkable efficiency in applications such as monitoring of material deformation, acoustic attenuation and energy storage. Moreover, neither expensive materials nor complex equipment were required for the composite manufacturing process.* We anticipate this work to make an important contribution to the development of porous functional materials for broad applications in scientific research and engineering.

Acknowledgments

QM and JM thank Asbury (Asbury, NJ, USA) for providing the GIC (1721). This work was financially supported by the the Natural Science Foundation of Liaoning Province (2019-MS-256), Aeronautical Science Foundation of China (2018ZF54036), China Postdoctoral Science Foundation (2019M651151), National Natural Science Foundation (51973123) and the plan of rejuvenating the talents of Liaoning province (XLYC1907135). JM thanks financial support by the Australian Research Council (DP200101737).

Reference

1. Suo, L., et al., *Hard carbon spheres interconnected by carbon nanotubes as high-performance anodes for sodium-ion batteries.* Carbon, 2019. **151**: p. 1-9.
2. Jeyaranjan, A., et al., *Scalable ternary hierarchical microspheres composed of PANI/ rGO/CeO2 for high performance supercapacitor applications.* Carbon, 2019. **151**: p. 192-202.
3. Ruan, C. and M. Chen, *Hierarchical carbon nanotube/nanocapsule composite via a facile arc discharge approach for high-frequency microwave absorption.* Materials Letters, 2019. **249**: p. 87-90.
4. Oh, Y.J., J.H. Kim, and Y.C. Kang, *Yolk–shell-structured manganese oxide/nitride composite powders comprising cobalt-nanoparticle-embedded nitrogen-doped carbon nanotubes as cathode catalysts for long-life-cycle lithium–oxygen batteries.* Chemical Engineering Journal, 2019. **373**: p. 86-94.
5. Mao, Y., et al., *Improving the lithium storage performance of SnO2 nanoparticles by in-situ embedding into a porous carbon framework.* Journal of Alloys and Compounds, 2019. **803**: p. 224-230.
6. Zhao, Y., et al., *3D-structured multi-walled carbon nanotubes/copper nanowires composite as a porous current collector for the enhanced silicon-based anode.* Journal of Alloys and Compounds, 2019. **803**: p. 505-513.
7. Liu, Y., et al., *Biomass-Swelling Assisted Synthesis of Hierarchical Porous Carbon Fibers for Supercapacitor Electrodes.* ACS Appl Mater Interfaces, 2016. **8**(42): p. 28283-28290.
8. Wang, L., et al., *MOF-derived NiO/Ni architecture encapsulated into N-doped carbon nanotubes for advanced asymmetric supercapacitors.* Inorganic Chemistry Frontiers, 2019. **6**(6): p. 1553-1560.
9. Xu, T., et al., *Design of the seamless integrated C@NiMn-OH-Ni3S2/Ni foam advanced electrode for supercapacitors.* Chemical Engineering Journal, 2019. **362**: p. 783-793.
10. Shin, D., et al., *Sol-gel-driven combustion wave for scalable transformation of Mn(NO3)2 precursors into MnO2-X/MWCNT supercapacitor electrodes capable of electrochemical activation.* Carbon, 2019. **152**: p. 746-754.
11. Ebrahimi, S., A. Shakeri, and T. Alizadeh, *Thermal Decomposition of Ammonium Perchlorate in the Presence of Cobalt Hydroxyl@Nano-Porous Polyaniline.* Journal of Inorganic and Organometallic Polymers and Materials, 2019. **29**(5): p. 1716-1727.
12. Yao, R.-q., X.-y. Lang, and Q. Jiang, *Recent advances of nanoporous metal-based catalyst: synthesis, application and perspectives.* Journal of Iron and Steel Research International, 2019. **26**(8): p. 779-

795.
13. Zhong, Y., et al., *Three-dimensional MoS2/Graphene Aerogel as Binder-free Electrode for Li-ion Battery.* Nanoscale Res Lett, 2019. **14**(1): p. 85.
14. Zhu, Q., et al., *Confined Growth of Nano-Na3V2(PO4)3 in Porous Carbon Framework for High-Rate Na-Ion Storage.* ACS Appl Mater Interfaces, 2019. **11**(3): p. 3107-3115.
15. Yan, Y., et al., *3D phosphorus-carbon electrode with aligned nanochannels promise high-areal-capacity and cyclability in lithium-ion battery.* Applied Surface Science, 2019. **489**: p. 734-740.
16. Geuli, O., Q. Hao, and D. Mandler, *One-step fabrication of NiOx-decorated carbon nanotubes-NiCo2O4 as an advanced electroactive composite for supercapacitors.* Electrochimica Acta, 2019. **318**: p. 51-60.
17. Yan, J., et al., *The 3D CoNi alloy particles embedded in N-doped porous carbon foams for high-performance microwave absorbers.* Carbon, 2019. **152**: p. 545-555.
18. Zhou, J., et al., *Silk fibroin-graphene oxide functionalized melamine sponge for efficient oil absorption and oil/water separation.* Applied Surface Science, 2019. **497**.
19. Nayl, A.A., et al., *Development of sponge/graphene oxide composite as eco-friendly filter to remove methylene blue from aqueous media.* Applied Surface Science, 2019. **496**.
20. Li, C., et al., *A sustainable construction of an efficient lightweight microwave absorber from polymeric sponge.* Ceramics International, 2019. **45**(15): p. 18572-18582.
21. Cao, Y., et al., *Mussel-inspired Ag nanoparticles anchored sponge for oil/water separation and contaminants catalytic reduction.* Separation and Purification Technology, 2019. **225**: p. 18-23.
22. Xu, H., et al., *A 3D porous NCNT sponge anode modified with chitosan and Polyaniline for high-performance microbial fuel cell.* Bioelectrochemistry, 2019. **129**: p. 144-153.
23. Zhang, Y., et al., *Facile Preparation of ZIF-67 Coated Melamine Sponge for Efficient Oil/Water Separation.* Industrial & Engineering Chemistry Research, 2019. **58**(37): p. 17380-17388.
24. Meng, Q., et al., *Flexible strain sensors based on epoxy/graphene composite film with long molecular weight curing agents.* Journal of Applied Polymer Science, 2019. **136**(35).
25. Han, S., et al., *Mechanical and electrical properties of graphene and carbon nanotube reinforced epoxy adhesives: Experimental and numerical analysis.* Composites Part A: Applied Science and Manufacturing, 2019. **120**: p. 116-126.
26. Meng, Q., et al., *A facile approach to fabricate highly sensitive, flexible strain sensor based on elastomeric/graphene platelet composite film.* Journal of Materials Science, 2019. **54**(15): p. 10856-10870.
27. Alam, A., et al., *Electrically conductive, mechanically robust, pH-sensitive graphene/polymer composite hydrogels.* Composites Science and Technology, 2016. **127**: p. 119-126.
28. Mei, X., et al., *An ultra-thin carbon-fabric/graphene/poly(vinylidene fluoride) film for enhanced electromagnetic interference shielding.* Nanoscale, 2019. **11**(28): p. 13587-13599.
29. Sun, X., et al., *A flexible graphene–carbon fiber composite electrode with high surface area-normalized capacitance.* Sustainable Energy & Fuels, 2019. **3**(7): p. 1827-1832.
30. Peng, M., et al., *Synthesis and application of modified commercial sponges for oil-water separation.* Chemical Engineering Journal, 2019. **373**: p. 213-226.
31. Wang, Y., et al., *Solar-heated graphene sponge for high-efficiency clean-up of viscous crude oil spill.* Journal of Cleaner Production, 2019. **230**: p. 995-1002.
32. Ma, Z., et al., *Lightweight, compressible and electrically conductive polyurethane sponges coated with synergistic multiwalled carbon nanotubes and graphene for piezoresistive sensors.* Nanoscale, 2018.

10(15): p. 7116-7126.
33. Zhao, L., et al., *Construction of sandwich-like porous structure of graphene-coated foam composites for ultrasensitive and flexible pressure sensors.* Nanoscale, 2019. **11**(21): p. 10229-10238.
34. Meng, Q., et al., *Toughening polymer adhesives using nanosized elastomeric particles.* Journal of Materials Research, 2014. **29**(5): p. 665-674.
35. Zhai, Y., et al., *Flexible and wearable carbon black/thermoplastic polyurethane foam with a pinnate-veined aligned porous structure for multifunctional piezoresistive sensors.* Chemical Engineering Journal, 2020. **382**.
36. Chen, W., et al., *Facile Fabrication of Multifunctional Polymer Composites Based on Three-Dimensional Interconnected Networks of Graphene and Carbon Nanotubes.* Industrial & Engineering Chemistry Research, 2019. **58**(47): p. 21531-21541.
37. Zhao, X., et al., *Highly Conductive Multifunctional rGO/CNT Hybrid Sponge for Electromagnetic Wave Shielding and Strain Sensor.* Advanced Materials Technologies, 2019. **4**(9).
38. Passaretti, P., et al., *Multifunctional graphene oxide-bacteriophage based porous three-dimensional micro-nanocomposites.* Nanoscale, 2019. **11**(28): p. 13318-13329.
39. Lu, Y., Z. Niu, and W. Yuan, *Multifunctional magnetic superhydrophobic carbonaceous aerogel with micro/nano-scale hierarchical structures for environmental remediation and energy storage.* Applied Surface Science, 2019. **480**: p. 851-860.
40. Araby, S., et al., *Graphene platelets versus phosphorus compounds for elastomeric composites: flame retardancy, mechanical performance and mechanisms.* Nanotechnology, 2019. **30**(38): p. 385703.
41. Meng, Q., et al., *Effect of interface modification on PMMA/graphene nanocomposites.* Journal of Materials Science, 2014. **49**(17): p. 5838-5849.
42. Qiang, F., et al., *Facile synthesis of super-hydrophobic, electrically conductive and mechanically flexible functionalized graphene nanoribbon/polyurethane sponge for efficient oil/water separation at static and dynamic states.* Chemical Engineering Journal, 2018. **334**: p. 2154-2166.
43. Yao, H.B., et al., *A flexible and highly pressure-sensitive graphene-polyurethane sponge based on fractured microstructure design.* Adv Mater, 2013. **25**(46): p. 6692-8.
44. Zhang, S., et al., *Conductive shear thickening gel/polyurethane sponge: A flexible human motion detection sensor with excellent safeguarding performance.* Composites Part A: Applied Science and Manufacturing, 2018. **112**: p. 197-206.
45. Zhou, S., et al., *One-pot synthesis of robust superhydrophobic, functionalized graphene/polyurethane sponge for effective continuous oil–water separation.* Chemical Engineering Journal, 2016. **302**: p. 155-162.
46. Sun, S., et al., *A wearable strain sensor based on the ZnO/graphene nanoplatelets nanocomposite with large linear working range.* Journal of Materials Science, 2019. **54**(9): p. 7048-7061.
47. Meng, Q., et al., *Non‐oxidized graphene/elastomer composite films for wearable strain and pressure sensors with ultra‐high flexibility and sensitivity.* Polymers for Advanced Technologies, 2019. **31**(2): p. 214-225.
48. Huang, J., et al., *Flexible electrically conductive biomass-based aerogels for piezoresistive pressure/strain sensors.* Chemical Engineering Journal, 2019. **373**: p. 1357-1366.
49. Carvalho, A.F., et al., *Laser-Induced Graphene Strain Sensors Produced by Ultraviolet Irradiation of Polyimide.* Advanced Functional Materials, 2018. **28**(52).
50. Su, X., et al., *3D Porous Superhydrophobic CNT/EVA Composites for Recoverable Shape Reconfiguration and Underwater Vibration Detection.* Advanced Functional Materials, 2019. **29**(24).

51. Moussa, M., et al., *Development of flexible supercapacitors using an inexpensive graphene/PEDOT/MnO 2 sponge composite.* Materials & Design, 2017. **125**: p. 1-10.
52. Cao, N., et al., *Polyurethane sponge functionalized with superhydrophobic nanodiamond particles for efficient oil/water separation.* Chemical Engineering Journal, 2017. **307**: p. 319-325.
53. Ma, C.Y. and C.H. Hou, *Enhancing the water desalination and electricity generation of a microbial desalination cell with a three-dimensional macroporous carbon nanotube-chitosan sponge anode.* Sci Total Environ, 2019. **675**: p. 41-50.
54. Ge, G., et al., *A flexible pressure sensor based on rGO/polyaniline wrapped sponge with tunable sensitivity for human motion detection.* Nanoscale, 2018. **10**(21): p. 10033-10040.
55. Cao, C.-F., et al., *Design of mechanically stable, electrically conductive and highly hydrophobic three-dimensional graphene nanoribbon composites by modulating the interconnected network on polymer foam skeleton.* Composites Science and Technology, 2019. **171**: p. 162-170.
56. Xu, H., et al., *Temperature-triggered sensitive resistance transition of graphene oxide wide-ribbons wrapped sponge for fire ultrafast detecting and early warning.* J Hazard Mater, 2019. **363**: p. 286-294.